

Heng LIU, Jie HONG, Dayi ZHANG

Bending and vibration of a discontinuous beam with a curvic coupling under different axial forces

© The Author(s) 2020. This article is published with open access at link.springer.com and journal.hep.com.cn

Abstract The transverse stiffness and vibration characteristics of discontinuous beams can significantly differ from those of continuous beams given that an abrupt change in stiffness may occur at the interface of the former. In this study, the equations for the deflection curve and vibration frequencies of a simply supported discontinuous beam under axial loads are derived analytically on the basis of boundary, continuity, and deformation compatibility conditions by using equivalent spring models. The equation for the deflection curve is solved using undetermined coefficient methods. The normal function of the transverse vibration equation is obtained by separating variables. The differential equations for the beam that consider moments of inertia, shearing effects, and gyroscopic moments are investigated using the transfer matrix method. The deflection and vibration frequencies of the discontinuous beam are studied under different axial loads and connection spring stiffness. Results show that deflection decreases and vibration frequencies increase exponentially with increasing connection spring stiffness. Moreover, both variables remain steady when connection spring stiffness reaches a considerable value. Lastly, an experimental study is conducted to investigate the vibration characteristics of a discontinuous beam with a curvic coupling, and the results exhibit a good match with the proposed model.

Keywords discontinuous beam, bending stiffness, transverse vibration, axial loads, gyroscopic moments

Received October 6, 2019; accepted December 24, 2019

Heng LIU, Jie HONG, Dayi ZHANG (✉)
School of Energy and Power Engineering, Beihang University, Beijing 100191, China
E-mail: dayi@buaa.edu.cn

Heng LIU
State Key Laboratory of Laser Propulsion and Application, Beijing Power Machinery Institute, Beijing 100074, China

1 Introduction

The mechanical structure of an aeroengine rotor can be simplified as a structural system that consists of multi-section beams and connecting structures. The multi-section beams in the rotor are typically defined as a discontinuous beam [1]. The deflection of continuous beams can be easily obtained via the classical principles of material mechanics [2]. However, given that a discontinuous beam has physical contact interfaces that cause discontinuities in mechanical properties, an abrupt change in stiffness may occur and result in complexity in predicting the bending and vibration of a discontinuous beam [3–6].

Various models have been developed to simulate the bending and vibration of continuous Euler–Bernoulli and Timoshenko beams. Han et al. [7] developed a mechanical model that considered damping to analyze a double-beam system with a viscoelastic connection layer. The governing differential equation was formulated on the basis of Euler–Bernoulli beam theory [8], and the effects of structural parameters on the modal and damping characteristic of the double-beam system were subsequently studied [9]. Han et al. [10] also proposed a unified dynamic analysis method for modeling complex cable systems, such as a shallow sagged cable system, in which the transcendental function of frequency was solved by adopting an improved Wittrick–Williams algorithm [11]. Paunović et al. [12] presented an approach for solving the vibration problem of fractionally damped beams with concentrated masses and base excitation. The solution was verified against an exact solution and a solution that used the finite element method (FEM), and the comparison exhibited good agreement. Wu and Chang [13] determined the exact solutions for the free vibrations of a nonuniform beam with concentrated masses using the continuous-mass transfer matrix method (TMM), accounting for shear deformation, rotary inertia, and axial load. The results were also compared with solutions that used FEM, and good agreements were shown. Lin [14] studied the frequency response amplitudes of a multiple-span beam with concentrated elements by using the

numerical assembly method. Hong and Kim [15] proposed a modal analysis method for multispan uniform Timoshenko beam structures supported or connected by joints with damping, and the exact solution for frequency was derived. However, existing methods that help determine the frequency of continuous beams cannot be fully applied to discontinuous beams because of the difference between the two types of beams.

The interest in the bending and vibration of discontinuous beams has increased in recent years. Yuan et al. [16] simplified a connection structure into an equivalent stiffness model by introducing a mass-free, hinge-bending spring to model stiffness weakening and developed an improved 2D FEM program to account for contact effects. Chenaghlou et al. [17,18] proposed a semirigid connection model of a joint system based on experimental results and subsequently studied the interaction between compressive axial force and bending moment using FEM. Yuan et al. [19] adopted FEM with very fine meshes to directly model a discontinuous beam with curvic couplings; however, the influence of axial loads was not considered. Liu et al. [20] established 3D finite element models of bolted and spline joints to analyze their local stiffness, and the solutions were verified against their experimental results. In the preceding studies, FEM was used to analyze the stiffness characteristics of connection structures. In engineering design, however, analytical or semianalytical methods are more direct and effective for assessing the influences of parameters on the bending and vibration of discontinuous beams. Failla et al. [21–25] presented a systematic study on the deformation and vibration of a Euler–Bernoulli discontinuous beam based on Green’s functions, in which closed-form solutions were obtained. However, the effects of axial loads, shearing, and gyroscopic moments were not included in their work. Hei et al. [26] introduced spring elements to model the stiffness weakening of a rod-fastening rotor supported by fixed-tilting pad journal bearings. The nonlinear unbalanced responses of the rotor–bearing system were obtained using a self-adaptive Runge–Kutta method. Although the aforementioned studies provide insight into the bending and vibration of discontinuous beams, limited studies on the development of analytical models for discontinuous beams with curvic couplings are found in the literature.

Curvic couplings, which differ from arc tooth face gears [27,28], are composed of convex and concave teeth. Gleason Corporation, US has been developing a theory for the structural design of curvic couplings since the 1940s [29]. With the application of Gleason Corporation’s grinding machines for curvic couplings, the analytical model developed by Gleason Corporation has been widely used in the turbomachinery industry. In a typical curvic coupling of a beam, the teeth are located at the end faces of the beam, exhibiting a hub-and-spoke pattern. The shape of tooth surfaces is part of a cone, and the cross section of a tooth along the radius of the beam is trapezoidal. Face-to-

face contacts are established when meshing convex and concave teeth. To ensure stable connections, sufficient axial preloads must be provided [30]. Preloads are provided in two ways: Connection with equally spaced and preloaded rods on the circumference of the beam and connection with a preloaded rod through the bore of the beam.

Existing mechanical models for analyzing the bending and vibration of beams are mostly established on the basis of Euler–Bernoulli and Timoshenko beams. Analytical methods, such as FEM, TMM [31,32], and dynamic stiffness methods [33], are generally adopted to solve these models. An analytical method exhibits the advantage of high precision, but it is not applicable to complex mechanical models, such as a model that simultaneously considers axial and shearing forces. FEM can solve complex mechanical models with high accuracy, but calculation efficiency can be an issue when considering contact effects in complex structures. Compared with FEM, the advantage of using TMM is that the dimension of the matrix increases slightly with an increase in the degree of freedom of a structure system. TMM also exhibits good modeling efficiency, a simple program design, and less memory occupation. Furthermore, TMM is also applicable to the analysis of rotor dynamics, wherein the beam model is compatible with that in gas turbine engineering.

Most aeroengine rotor systems are designed to be discontinuous structures with couplings [34]. The difficulty in the design of a discontinuous rotor is the modeling of dynamic behavior. Existing models for vibration analysis have several shortcomings, such as lack of boundary conditions and low calculation efficiency. These shortcomings affect efficiency and accuracy in rotor design. The purpose of the current study is to establish a model that involves the complete boundary conditions for predicting the transverse bending and vibration of a discontinuous beam with curvic couplings. A semianalytical method is presented to simulate the transverse bending and vibration characteristics of a simply supported discontinuous beam under axial loads and rotation speed by considering shearing and gyroscopic effects. An approximate equation for deflection curve and a partial differential equation for transverse vibration are derived based on Timoshenko beam theory, and the corresponding solutions for the deflection and vibration frequencies are provided by adopting the undetermined coefficient and TMMs, respectively. The influence of connection stiffness on vibration frequencies is demonstrated in the modeling of a typical example of a discontinuous beam with a curvic coupling. A finite element analysis of curvic coupling that considers contact effects is also conducted to correct connection stiffness. Lastly, a modal experiment is performed using the multipoint excitation and vibration pickup method, and the experimental results exhibit good agreement with the solutions obtained using the proposed model.

2 Basic assumptions

The jointed structures of gas turbine rotors are classified into spline joints, bolted flange joints, and curvic couplings [34]. This study focuses on the deformation and vibration characteristics of a discontinuous beam with curvic coupling, as shown in Fig. 1. A beam of annular sections is cut into two segments. One end of each segment is machined into curvic teeth. The two segments are connected via curvic coupling under axial loads, which are provided by a slender tie rod through bores.

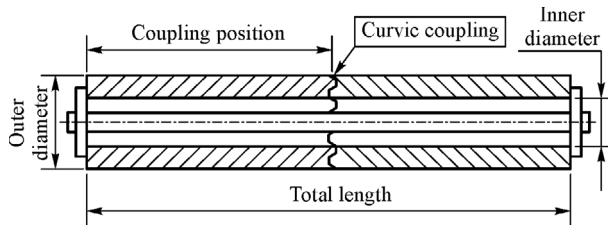


Fig. 1 Discontinuous beam with the curvic coupling.

Several scholars have proposed simplified stiffness models for these connection structures, such as the equivalent spring model [6,35] and the virtual material model [36]. The equivalent spring model, which uses spring elements to represent the stiffness characteristics of connections, is widely used in calculating the stiffness of discontinuous beams. The basic assumptions of this study are presented in accordance with the aforementioned literature:

- a) The connection structures of a discontinuous beam are simplified using springs with torsion and shearing stiffness;
- b) The stiffness of springs is linear;
- c) Timoshenko beam theory is adopted;
- d) The direction of axial load does not change with the bending of the beam;
- e) The large deflection effect is disregarded;
- f) The effect of the tie rod is disregarded; and
- g) Variable units are international units unless otherwise specified. They are m, kg, N, rad, and s for length, mass, force, radian, and time, respectively.

3 Bending stiffness of the discontinuous beam

A simply supported discontinuous beam with length l has a connection structure at distance m from its left end. The length of the connection structure is considerably shorter than that of the beam, which can be simplified as a connection point. Referring to previous statements, the connection structure can be simplified as a torsion spring

with stiffness k_t and a shearing spring with stiffness k_s . A transverse force F is applied at distance a , and an axial force F_N , whose direction is normal to the cross section of the beam, is applied at the right end of the beam, as shown in Fig. 2. The beam has a total deflection w_d . In accordance with Timoshenko theory, the deflection and slope caused by bending and shearing can be represented by w_b , θ_b , w_s , and θ_s , respectively.

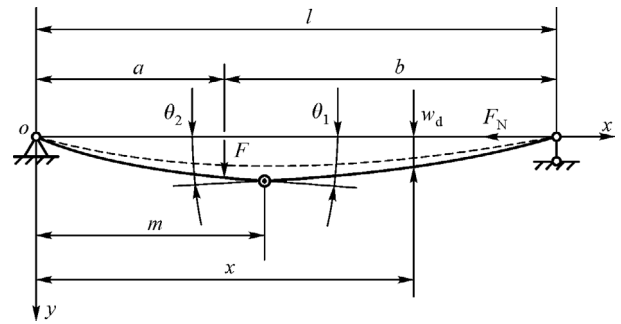


Fig. 2 Illustration of the bending deflection of the discontinuous beam.

These parameters exhibit the following relationships

$$w_d = w_b + w_s, \tag{1}$$

$$w'_d = w'_b + w'_s, \tag{2}$$

where ' represents the first derivative of variables.

Here, w_1 and w_2 represent the deflections of the two segments at m .

$$w_1 - w_2 = \frac{F_s(m)}{k_s}, \tag{3}$$

where F_s is the shearing force of a transverse section of the beam.

The notations θ_1 and θ_2 represent the slopes of the two segments at m .

$$\theta_1 - \theta_2 = \frac{M(m)}{k_t}, \tag{4}$$

where M is the bending moment of a transverse section of the beam.

The approximate differential equation that represents the relationship between forces and deformations for the simply supported discontinuous beam with axial and transverse loads is derived as [37]

$$M + F_N w_d = -EI_z \frac{d\theta_b}{dx}, \tag{5}$$

where E is Young's modulus, and I_z is the sectional moment of inertia.

Substituting Eq. (1) into Eq. (5) yields

$$EI_z w_b'' = \begin{cases} -\frac{Fb}{l}x - F_N(w_b + w_s) & x \in [0, a], \\ -\frac{Fa}{l}(l-x) - F_N(w_b + w_s) & x \in (a, l], \end{cases} \quad (6)$$

where "'' represents the second derivative of variables.

Let

$$\kappa^2 = \frac{F_N}{EI_z}. \quad (7)$$

Its general solution is in the form

$$w_d = \begin{cases} A_1 \cos(\kappa x) + A_2 \sin(\kappa x) - \frac{Fbx}{F_N l} & x \in [0, a), \\ B_1 \cos(\kappa x) + B_2 \sin(\kappa x) - \frac{Fa}{F_N l}(l-x) & x \in [a, m), \\ C_1 \cos(\kappa x) + C_2 \sin(\kappa x) - \frac{Fa}{F_N l}(l-x) & x \in (m, l], \end{cases} \quad (8)$$

where $A_1, A_2, B_1, B_2, C_1,$ and C_2 are undetermined coefficients. Notably, w_d is discontinuous at point m because the definition domain does not include this point.

In accordance with the connection conditions at point m , the following conditions should be satisfied:

$$w_b(0) = w_b(l) = 0, \quad (9a)$$

$$w_b(a^-) = w_b(a^+), \quad (9b)$$

$$w_b(m^-) - w_b(m^+) = w_1 - w_2, \quad (9c)$$

$$w_b'(m^-) - w_b'(m^+) = \theta_1 - \theta_2, \quad (9d)$$

$$w_b'(a^-) = w_b'(a^+), \quad (9e)$$

where the superscripts "−" and "+" represent the left and right limits of arguments, respectively.

The unknown coefficients in Eq. (8) are identified using the undetermined coefficient method and are listed as follows:

$$A_1 = 0, \quad (10a)$$

$$A_2 = \frac{F \sin[\kappa(l-m)]}{lk_t \kappa \sin(\kappa l)}(l-x) + \frac{F \sin(\kappa b)}{\kappa \sin(\kappa l)} \left(\frac{1}{F_N} + \frac{f_s}{GA} \right) + \frac{F \cos[\kappa(l-m)]}{lk_s \sin(\kappa l)}, \quad (10b)$$

$$B_1 = \frac{F \sin(\kappa a)}{\kappa} \left(\frac{1}{F_N} + \frac{f_s}{GA} \right), \quad (10c)$$

$$B_2 = \frac{F \sin[\kappa(l-m)]}{lk_t \kappa \sin(\kappa l)}(l-x) - \frac{F \sin(\kappa a) \cos(\kappa l)}{\kappa \sin(\kappa l)} \left(\frac{1}{F_N} + \frac{f_s}{GA} \right) + \frac{F \cos[\kappa(l-m)]}{lk_s \sin(\kappa l)}, \quad (10d)$$

$$C_1 = \frac{F \sin(\kappa m)}{lk_t \kappa}(l-x) + \frac{F \sin(\kappa a)}{\kappa} \left(\frac{1}{F_N} + \frac{f_s}{GA} \right) - \frac{F \cos(\kappa m)}{lk_s}, \quad (10e)$$

$$C_2 = -\frac{Fa(l-x) \sin(\kappa m) \cos(\kappa l)}{lk_t \kappa \sin(\kappa l)} - \frac{F \sin(\kappa a) \cos(\kappa l)}{\kappa \sin(\kappa l)} \left(\frac{1}{F_N} + \frac{f_s}{GA} \right) + \frac{F \cos(\kappa m) \cos(\kappa l)}{lk_s \sin(\kappa l)}, \quad (10f)$$

where f_s is the shear coefficient, G is the shear modulus, and A is the sectional area.

By substituting Eq. (10) into Eq. (8), the stiffness of the discontinuous beam is derived as follows:

$$k_d = \frac{F}{w_d}. \quad (11)$$

4 Vibration of the discontinuous beam

A beam segment under bending moment M , shearing force F_s , and axial force F_N is illustrated in Fig. 3. The transverse deformation of the beam, $w(x, t)$, can be expressed as

$$\begin{cases} \frac{\partial F_s}{\partial x} dx - \rho A \frac{\partial^2 w}{\partial t^2} dx = 0, \\ -\frac{\partial M}{\partial x} dx + F_s dx - \rho I_z \frac{\partial^2 \theta_b}{\partial t^2} dx + F_N \frac{\partial w}{\partial x} dx = 0, \end{cases} \quad (12)$$

where ρ is the density of the material. The second-order terms of dx are omitted because they are considerably less than dx .

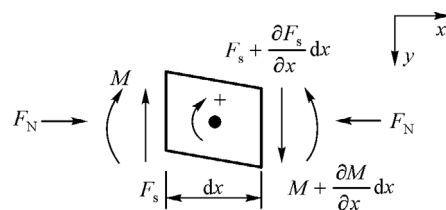


Fig. 3 Illustration of the inner forces of a beam segment.

The relationship between bending moment and its slope is

$$M = -EI_z \frac{d\theta_b}{dx}. \quad (13)$$

Given that

$$w = w_s + w_b, \quad (14)$$

the relationship between shearing force and its slope is

$$F_s = \frac{GA}{f_s} \left(\frac{\partial w}{\partial x} - \theta_b \right). \quad (15)$$

Substituting Eq. (15) into Eq. (12) derives

$$\begin{cases} \frac{\partial \theta_b}{\partial x} = \frac{\partial^2 w}{\partial x^2} - \frac{\rho f_s}{G} \frac{\partial^2 w}{\partial t^2}, \\ -\frac{\partial^2 M}{\partial x^2} + \rho A \frac{\partial^2 w}{\partial t^2} - \rho I_z \frac{\partial^3 \theta_b}{\partial x \partial t^2} + F_N \frac{\partial^2 w}{\partial x^2} = 0. \end{cases} \quad (16)$$

By eliminating θ_b , the differential equation is obtained as follows:

$$\begin{aligned} EI_z \frac{\partial^4 w}{\partial x^4} + \rho A \frac{\partial^2 w}{\partial t^2} - \rho I_z \left(\frac{f_s E}{G} + 1 \right) \frac{\partial^4 w}{\partial x^2 \partial t^2} \\ + \frac{\rho^2 I_z f_s}{G} \frac{\partial^4 w}{\partial t^4} + F_N \frac{\partial^2 w}{\partial x^2} \\ = 0. \end{aligned} \quad (17)$$

Although the solution method of Eq. (17) for continuous beams has been proposed in Ref. [31], solving it directly is difficult due to the discontinuity at m . Therefore, using the variable separation method is necessary to determine the solution.

The separation of variables is assumed in the form

$$w(x,t) = X(x)e^{j\omega t}, \quad (18)$$

where j is the square root of -1 .

Substituting Eq. (18) into Eq. (17) yields

$$X^{(4)} + (q+r+t)X^{(2)} - (s-rt)X = 0, \quad (19)$$

where superscripts “(2)” and “(4)” represent the second and fourth derivatives of variables, respectively.

$$q = \frac{F_N}{EI_z}, \quad r = \frac{\rho\omega^2}{E}, \quad s = \frac{\rho A\omega^2}{EI_z}, \quad t = \frac{\rho f_s\omega^2}{G}, \quad (20)$$

where ω is the angular velocity. The vibration frequency is f and $f = \omega/(2\pi)$.

The characteristic equation of Eq. (19) is

$$\lambda^4 + (q+r+t)\lambda^2 - (s-rt) = 0. \quad (21)$$

Let

$$p = \sqrt{(q+r)^2 + 2t(q-r) + t^2 + 4s}. \quad (22)$$

The eigenvalues are

$$\lambda_{1,2} = \pm k_1, \quad \lambda_{3,4} = \pm jk_2, \quad (23)$$

where

$$k_1 = \sqrt{\frac{p-(q+r+t)}{2}}, \quad k_2 = \sqrt{\frac{p+(q+r+t)}{2}}. \quad (24)$$

The general solution for Eq. (18) can be expressed as

$$\begin{aligned} X(x) = A \cosh(k_1 x) + B \sinh(k_1 x) + C \cos(k_2 x) \\ + D \sin(k_2 x), \end{aligned} \quad (25)$$

where the coefficients A , B , C , and D can be determined using TMM.

Vector $\mathbf{W} = [w, \theta, M, F_s]$, components of which represent the deflection, slope, bending moment, and shearing force of a station, is defined. Suppose two stations, expressed by i and $i+1$, are found on each beam segment. The transfer matrix of the beam segment is obtained as

$$\mathbf{W}_{i+1} = \mathbf{T} \mathbf{W}_i, \quad (26)$$

and the elements of the transfer matrix \mathbf{T} are listed as follows:

$$T_{11} = \frac{k_2^2 \cosh(k_1 l_i) + k_1^2 \cos(k_2 l_i)}{k_1^2 + k_2^2}, \quad (27a)$$

$$T_{12} = \frac{k_2^3 \sinh(k_1 l_i) + k_1^3 \sin(k_2 l_i)}{(k_1^2 + k_2^2) k_1 k_2}, \quad (27b)$$

$$T_{13} = \frac{-\cosh(k_1 l_i) + \cos(k_2 l_i)}{EI_z (k_1^2 + k_2^2)}, \quad (27c)$$

$$T_{14} = \frac{-k_2 \sinh(k_1 l_i) + k_1 \sin(k_2 l_i)}{EI_z (k_1^2 + k_2^2) k_1 k_2}, \quad (27d)$$

$$T_{21} = \frac{[k_2 \sinh(k_1 l_i) - k_1 \sin(k_2 l_i)] k_1 k_2}{k_1^2 + k_2^2}, \quad (27e)$$

$$T_{22} = T_{11}, \quad (27f)$$

$$T_{23} = \frac{-k_1 \sinh(k_1 l_i) - k_2 \sin(k_2 l_i)}{EI_z (k_1^2 + k_2^2)}, \quad (27g)$$

$$T_{24} = T_{13}, \quad (27h)$$

$$T_{31} = \frac{EI_z [-\cosh(k_1 l_i) + \cos(k_2 l_i)] k_1^2 k_2^2}{k_1^2 + k_2^2}, \quad (27i)$$

$$T_{32} = \frac{EI_z [-k_2 \sinh(k_1 l_i) + k_1 \sin(k_2 l_i)] k_1 k_2}{k_1^2 + k_2^2}, \quad (27j)$$

$$T_{33} = \frac{k_1^2 \cosh(k_1 l_i) + k_2^2 \cos(k_2 l_i)}{k_1^2 + k_2^2}, \quad (27k)$$

$$T_{34} = \frac{k_1 \sinh(k_1 l_i) + k_2 \sin(k_2 l_i)}{k_1^2 + k_2^2}, \quad (27l)$$

$$T_{41} = \frac{EI_z[-k_1 \sinh(k_1 l_i) + k_2 \sin(k_2 l_i)]k_1^2 k_2^2}{k_1^2 + k_2^2}, \quad (27m)$$

$$T_{42} = T_{31}, \quad (27n)$$

$$T_{43} = \frac{k_1^3 \sinh(k_1 l_i) - k_2^3 \sin(k_2 l_i)}{k_1^2 + k_2^2}, \quad (27o)$$

$$T_{44} = T_{33}. \quad (27p)$$

The transfer matrix of the curvic coupling is

$$\begin{bmatrix} w \\ \theta \\ M \\ F_s \end{bmatrix}_R = \begin{bmatrix} 1 & 0 & 0 & -1/k_s \\ 0 & 1 & -1/k_t & 0 \\ 0 & 0 & 1 & 0 \\ 0 & 0 & 0 & 1 \end{bmatrix} \begin{bmatrix} w \\ \theta \\ M \\ F_s \end{bmatrix}_L. \quad (28)$$

where the subscripts “L” and “R” represent the left and right sections of curvic couplings, respectively.

Equation (28) is rewritten as

$$W_R = KW_L. \quad (29)$$

By adopting TMM, the deformation relationship at both ends of the beam segment is

$$W_n = T_n T_{n-1} \cdots K \cdots T_2 T_1 W_0, \quad (30)$$

which can be solved using the following conditions:

$$w(0,t) = w(l,t) = 0, \quad w''(0,t) = w''(l,t) = 0. \quad (31)$$

The frequency equation obtained from Eq. (30) is a transcendental equation. Finding an analytical solution for a transcendental equation is difficult, and thus, such equations should be solved using a numerical method. The Newton method [38] is adopted to solve Eq. (30). The

initial value of the example is estimated in accordance with the analytical solution for the frequency equation of a classical Euler–Bernoulli beam with the same size.

When the parameters of a simply supported discontinuous beam satisfy certain conditions, a relatively simple frequency equation can be obtained. Let $m = l/2$ and $k_s = \infty$, the frequency equation can be derived:

$$k_1^2 k_2 \tan \frac{k_2 l}{2} - k_1 k_2^2 \tanh \frac{k_1 l}{2} - \frac{2k_t(k_1^2 + k_2^2)}{EI_z} = 0, \quad (32)$$

$$\sinh \frac{k_1 l}{2} \sin \frac{k_2 l}{2} = 0.$$

5 Vibration of the discontinuous beam under rotation

If the beam illustrated in Fig. 2 is rotating around its x -axis, additional gyroscopic effects must be considered. The positive direction for the rotation of the beam segment is from the x -axis to the y -axis in the xoy plane, as illustrated in Fig. 3. Meanwhile, the direction is from the y -axis to the z -axis in the $yozy$ plane. Therefore, the relationships between bending moments and slopes are as follows:

$$M_z = -EI_z \frac{d\theta_z}{dx}, \quad (33)$$

$$M_y = EI_y \frac{d\theta_y}{dx}. \quad (34)$$

The relationships between shearing forces and slopes are as follows:

$$F_{sy} = \frac{GA}{f_s} \left(\frac{\partial w_y}{\partial x} - \theta_z \right), \quad (35)$$

$$F_{sz} = \frac{GA}{f_s} \left(\frac{\partial w_z}{\partial x} + \theta_y \right), \quad (36)$$

where subscripts y and z represent the directions of forces and moments and their corresponding deformations.

The equilibrium equations can be obtained as

$$\begin{cases} \frac{\partial F_{sy}}{\partial x} dx = \rho A \frac{\partial^2 w_y}{\partial t^2} dx, \\ -\frac{\partial M_z}{\partial x} dx + F_{sy} dx - \rho I_z \frac{\partial^2 \theta_z}{\partial t^2} dx + F_N \frac{\partial w_y}{\partial x} dx + \rho I_p \Omega \frac{\partial \theta_y}{\partial t} dx = 0, \\ \frac{\partial F_{sz}}{\partial x} dx = \rho A \frac{\partial^2 w_z}{\partial t^2} dx, \\ -\frac{\partial M_y}{\partial x} dx + F_{sz} dx + \rho I_y \frac{\partial^2 \theta_y}{\partial t^2} dx + F_N \frac{\partial w_z}{\partial x} dx + \rho I_p \Omega \frac{\partial \theta_z}{\partial t} dx = 0, \end{cases} \quad (37)$$

where Ω is the angular velocity of the beam, and I_p is the polar moment of inertia, which exhibits the relationship of $I_p = 2I_y = 2I_z$ for annular sections.

By using the complex coordinates [39]

$$u = w_y + jw_z, \tag{38}$$

where $j = \sqrt{-1}$.

substituting Eqs. (33)–(36) into Eq. (37), and eliminating θ_y and θ_z , the differential equations that consider axial loads, moments of inertia, shearing effects, and gyroscopic moments for rotation around the x -axis of the beam can be expressed as

$$\begin{aligned} EI_z \frac{\partial^4 u}{\partial x^4} + \rho A \frac{\partial^2 u}{\partial t^2} - \rho I_z \left(\frac{f_s E}{G} + 1 \right) \frac{\partial^4 u}{\partial x^2 \partial t^2} \\ + \frac{\rho^2 I_z f_s}{G} \frac{\partial^4 u}{\partial t^4} + F_N \frac{\partial^2 u}{\partial x^2} + j \rho I_p \Omega \left(\frac{\partial^3 u}{\partial x^2 \partial t} - \frac{\rho f_s}{G} \frac{\partial^3 u}{\partial t^3} \right) \\ = 0. \end{aligned} \tag{39}$$

Substituting Eq. (18) into Eq. (39) derives

$$X^{(4)} + (q + r + t - v)X^{(2)} - [s - t(r - v)]X = 0, \tag{40}$$

where

$$v = \frac{2\rho\Omega\omega}{E}. \tag{41}$$

Let

$$p = \sqrt{(q + r)^2 + (t + v)^2 + 2t(q - r) - 2v(q + r) + 4s}. \tag{42}$$

The eigenvalues of its characteristic equation are

$$\lambda_{1,2} = \pm k_1, \lambda_{3,4} = \pm jk_2, \tag{43}$$

where

$$\begin{aligned} k_1 &= \sqrt{\frac{p - (q + r + t - v)}{2}}, \\ k_2 &= \sqrt{\frac{p + (q + r + t - v)}{2}}. \end{aligned} \tag{44}$$

By using the same method presented in the previous chapter, the frequency equation for the discontinuous beam with the effects of axial loads, moments of inertia, shearing forces, and gyroscopic moments can be obtained. This equation is also a transcendental equation and can be solved using numerical methods.

6 Examples of deflection and vibration frequency analyses

The basic structural parameters and material properties of a

discontinuous beam are as follows: Total length $l = 0.88$ m, connection position $m = 0.44$ m, outer radius $R = 0.0205$ m, inner radius $r = 0.016$ m, Young's modulus $E = 2 \times 10^{11}$ Pa, Poisson's ratio $\nu = 0.3$, and mass density $\rho = 7850$ kg/m³. The value ranges of the shearing and torsion spring stiffness, i.e., $2 \times 10^5 - 2 \times 10^{10}$ N/m for shearing and $2 \times 10^5 - 2 \times 10^9$ N·m/rad for torsion, are given in accordance with the range of stiffness weakening ratio in engineering experiences. The deflection and vibration frequencies of a discontinuous beam under different connection stiffness values are analyzed using the proposed method.

6.1 Deflection analysis

The beam is under an axial load of $F_N = 2$ kN and a transverse load of $F = 5$ kN. The bending deflections of the beam with different torsion spring stiffness values are calculated while $a = 0.2$ m. The results are presented in Fig. 4. Compared with that of the beam without axial load, the transverse force considerably influences the deflection of the discontinuous beam when the torsion spring stiffness is small, and the deflection differences and the influence of axial loads on deflection decrease gradually with an exponential increase of the torsion spring stiffness. Considering shearing spring effects, the deflection curve shown in Fig. 5 can be obtained. Notably, an abrupt change occurs in the middle of the curve, and its relative deformation is subject to shearing spring stiffness.

Although torsion and shear spring decrease the stiffness of the discontinuous beam, the relationship between transverse force and deflection remains linear. Meanwhile, an increase in axial force increases the slope of the deflection curve.

6.2 Vibration frequency analysis

The vibration frequencies of the discontinuous beam

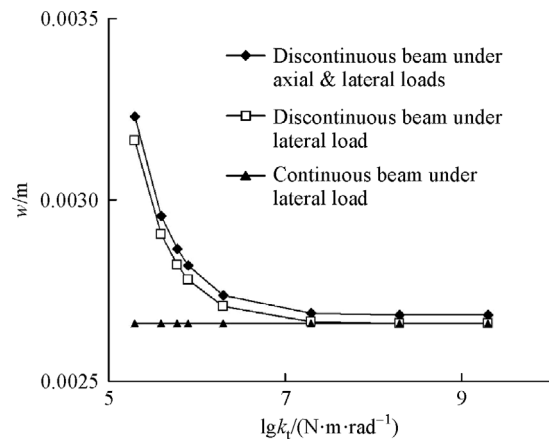


Fig. 4 Influence of axial loads and torsion spring stiffness on maximum beam deformations.

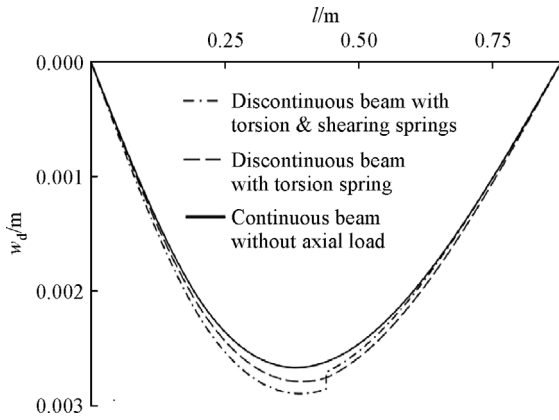


Fig. 5 Deflection curves of continuous and discontinuous beams.

without shearing spring effects are analyzed. When the stiffness of the torsion spring is the same, the frequency of each order decreases linearly with an increase in axial load, and the second- and fourth-order frequencies do not

change. This result is related to the fact that point m is located at the midpoint of the beam, as shown in Fig. 6(a). With an increase in torsion spring stiffness, the first- and third-order frequencies increase rapidly. When torsion spring stiffness reaches a certain value, the increase in frequency slows down and tends to become stable, as shown in Fig. 6(b).

Compared with Figs. 7(a) and 7(b), the trend of the third-order frequency is similar to that of the first-order frequency, but the frequency differences under the corresponding axial load are relatively small, indicating that the influence of the axial load on lower-order frequencies is greater, and the influence decreases gradually with an increase in frequency order. However, the influences of axial load on the first- and second-order frequencies of the beam are less than 4% and 1% within the full load range, respectively. Compared with the influence of stiffness weakening on frequencies, the influence of axial load is considered negligible.

The results that consider shearing spring effect are

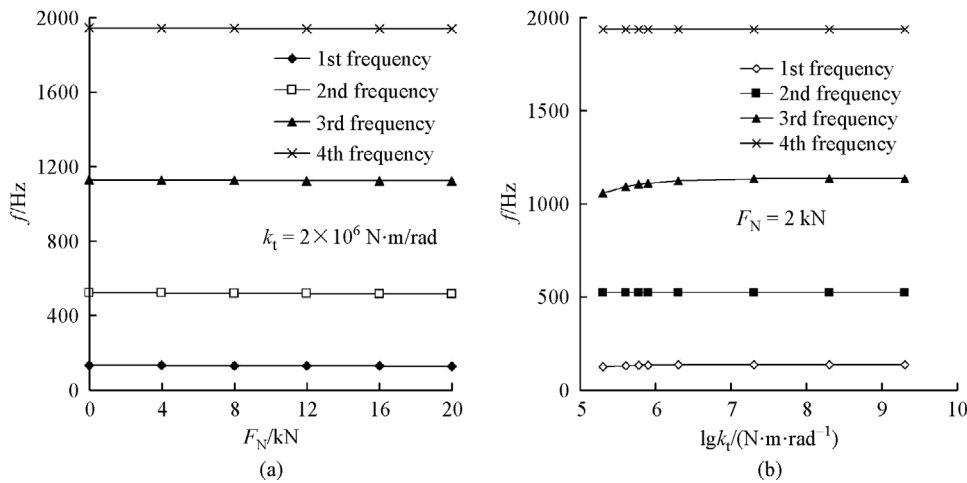


Fig. 6 First four frequencies of the discontinuous beam with (a) the same connection stiffness under different axial loads and (b) different torsion spring stiffness values under the same axial load.

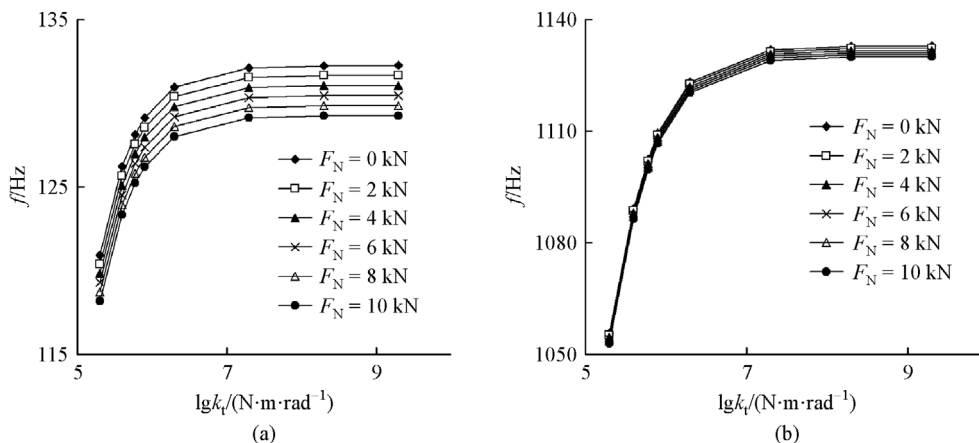


Fig. 7 Frequencies vs. torsion spring stiffness under different axial loads: (a) First- and (b) third-order frequencies.

shown in Fig. 8. When torsion spring stiffness is constant, the second- and fourth-order frequencies increase with an increase in shear spring stiffness. Meanwhile, the first- and third-order frequencies do not change, as shown in Fig. 8(a). The second-order frequency varies exponentially with shear spring stiffness, as shown in Fig. 8(b).

The effect of shear spring stiffness on frequencies is contrary to that of torsion spring stiffness. When the connection structure is located at the midpoint of the beam, an increase in shearing spring stiffness increases the even-order frequencies but does not change the odd-order frequencies. Meanwhile, an increase in torsion spring stiffness increases the odd-order frequencies but does not change the even-order frequencies. This phenomenon is attributed to the connection springs being located at the midpoint of the discontinuous beam and coinciding with the modal node of even-order modes. In the design of the example, the connection structure is placed in the middle of the beam to distinguish between the influences of torsion and shearing spring stiffness on frequencies with different orders. In this manner, the influences of torsion and shearing spring stiffness on frequencies can be observed directly.

7 Equivalent stiffness of curvic coupling

The configuration of curvic coupling is defined using the method proposed in Refs. [29,40], and the parameters are listed in Table 1. Curvic coupling is regarded as a separate segment that consists of concave and convex parts. The length of the segment is equal to the sum of the whole depth and clearances [29,40]. Then, 3D finite element

analysis of the adopted curvic coupling is performed using the commercial software ABAQUS while considering frictionless contact conditions. The elements outside the whole depth of teeth are considered fully constrained to the origin of the local coordinate system on their belonging part. External shearing and bending loads are applied to one part, and fixed constraints are applied to the other part. Stiffness is measured via the relative displacement of the two parts under given loads.

The maximum magnitudes of the applied shearing force and bending moment are 100 N and 30 N·m, respectively. A preload of 2 kN is applied to eliminate the influence caused by the alignment error of the elements on tooth surfaces, maintaining full engagement of the teeth in the analysis process. The shearing stiffness of curvic coupling is 4.655×10^9 N/m, and the torsion stiffness is 1.835×10^6 N·m/rad. The influence of shearing stiffness can be disregarded in this example because the frequency curves straighten out when shearing stiffness is sufficiently large, as shown in Fig. 8(a). Thus, torsion stiffness is used in the subsequent analysis.

Notably, a deviation exists between a finite element model and practice. The contact condition in finite element analysis is set to full engagement even if the axial force is small. However, not all teeth are fully engaged when the axial load is small because of machining errors of tooth surfaces.

8 Experimental verification

A continuous beam is fabricated from stainless steel in accordance with the total length and cross-section

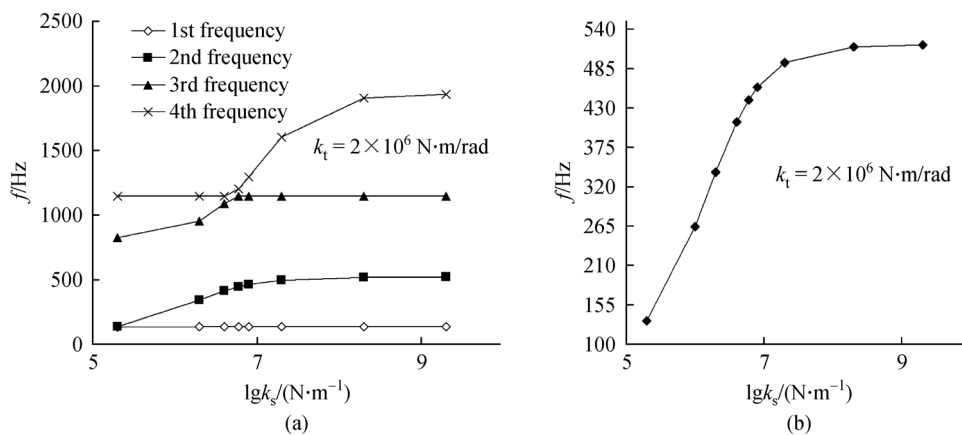


Fig. 8 Frequencies vs. shearing spring stiffness: (a) The first four frequencies and (b) detailed view of the second-order frequency.

Table 1 Parameters of curvic coupling

Outer diameter	Tangency radius	Tooth width	Tooth number	Enveloped half pitches	Pressure angle	Whole depth	Clearance
41 mm	18.25 mm	4.5 mm	12	11	40°	2.733 mm	0.41 mm

diameters mentioned earlier. Then, the beam is cut into two equal-length segments. One end face of each segment is machined into curvic couplings, which consist of convex teeth for one end and concave teeth for the other end. The two segments are connected via curvic coupling and tightened using a tie rod with threads through the bores. The beam is simply supported by interference-fitted flanges, which are mounted onto supporting structures with sufficient stiffness, as shown in Fig. 9.

The frequencies are measured using the multipoint excitation and vibration pickup method. The beam is marked with nine equally spaced points, which are considered excitation points. Two accelerometers are

placed at points #3 and #6. Signal monitoring and acquisition are achieved using the Data Acquisition and Signal Processing (DASP) system (Version 11) produced by China Orient Institute of Noise and Vibration, and sampling frequency is set to 5120 Hz. At least three groups of tests are conducted, and the results are consistent. The same test is performed on a continuous beam of the same size to eliminate system errors. The frequency domain method integrated into the DASP system, known as the PolyMAX method [41], is adopted to identify modal parameters. The diagram of the frequency response function is shown in Fig. 10. Given the existence of the tie rod, the spectrum measured includes its frequencies.

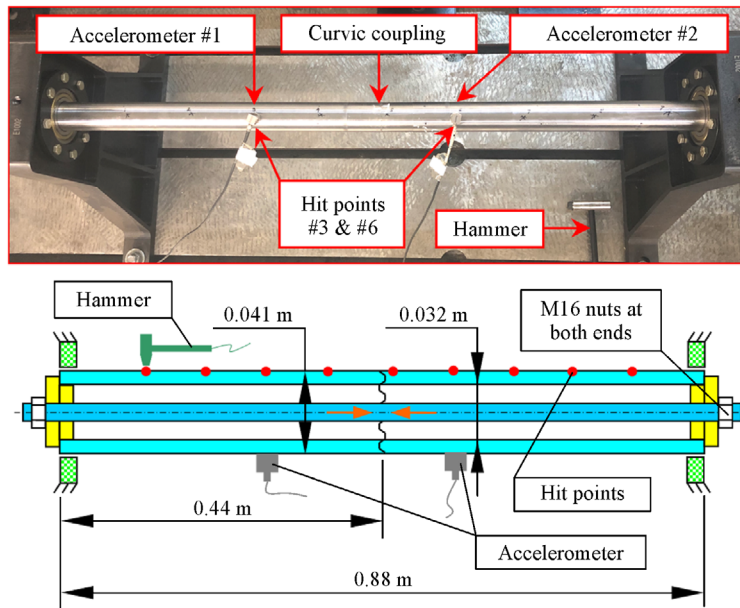


Fig. 9 Specimen for modal test.

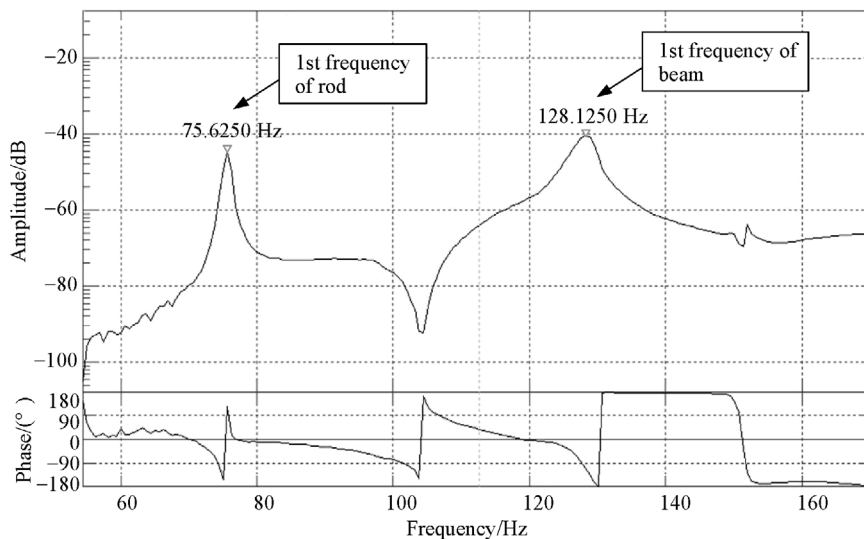


Fig. 10 Diagram of the frequency response function.

The vibration frequencies of the beam are identified by analyzing the mode responses of each order.

By comparing the calculated results of vibration frequencies under different stiffness values with the experimental data, the tested vibration frequencies are determined to be similar to the calculation results with torsion spring stiffness $k_t = 2 \times 10^6 \text{ N}\cdot\text{m}/\text{rad}$, as shown in Fig. 11(a). Frequencies vary considerably when the axial load is low because the low-level pretension reduces the stiffness of curvic coupling and decreases frequencies. By comparing the experimental data with the analytical solutions of the given variables, the trend of the first three-order frequencies is determined to be consistent, as shown in Fig. 11(b). The third-order frequency tested is less than the analytical solution, and the error is approximately 5%.

The comparison of the first- and third-order frequencies in Figs. 6(b) and 11 shows that the bending stiffness of the discontinuous beam with curvic coupling changes exponentially with axial load when the pretension level is low.

9 Conclusions

This study focuses on establishing a semianalytical approach for simulating the bending deflection and vibration frequencies of a simply supported discontinuous beam under axial loads and rotation speed along its longitudinal axis. Shearing and gyroscopic effects are considered, and the undetermined coefficient and TMMs are used in the solution process. The key conclusions can be summarized as follows.

1) A mechanical model for a simply supported discontinuous beam under axial loads accounting for bending and shearing stiffness weakening is proposed on

the basis of Timoshenko beam theory, and parametric studies are performed.

2) The influence of axial forces on lower-order frequencies is greater than on higher-order frequencies, and bending deflection and vibration frequencies are more sensitive to axial forces than stiffness weakening.

3) The results show an exponential increase in frequency when torsion spring stiffness increases. Meanwhile, an exponential increase in frequency is observed with increasing shearing spring stiffness.

4) A critical stiffness exists, below which bending deflection and vibration frequencies vary exponentially. Bending deflection and vibration tend to be stable when stiffness is above this critical value.

5) A zone exists before the critical stiffness is reached, wherein a narrow change in pretension force can lead to a significant decrease in the frequencies of the discontinuous beam with curvic coupling. This phenomenon help discover the abnormality of connection structures before the failure of curvic couplings.

6) The frequencies measured from the performed experiments exhibit good agreement with the predicted results using the proposed semianalytical method, demonstrating that the proposed method can be used in the practical design of aeroengine rotors with curvic couplings.

Acknowledgements The authors would like to acknowledge the financial support provided by the Ministry of Industry and Information Technology of China (Grant No. JSZL2016204B102) and the National Natural Science Foundation of China (Grant Nos. 51575022 and 11772022).

Open Access This article is licensed under Creative Commons Attribution 4.0 International License, which permits use, sharing, adaptation, distribution, and reproduction in any medium or format, as long as appropriate credit is given to the original author(s) and the source, a link is provided to the Creative Commons license, and any changes made are indicated.

Images or other third-party materials in this article are included in the

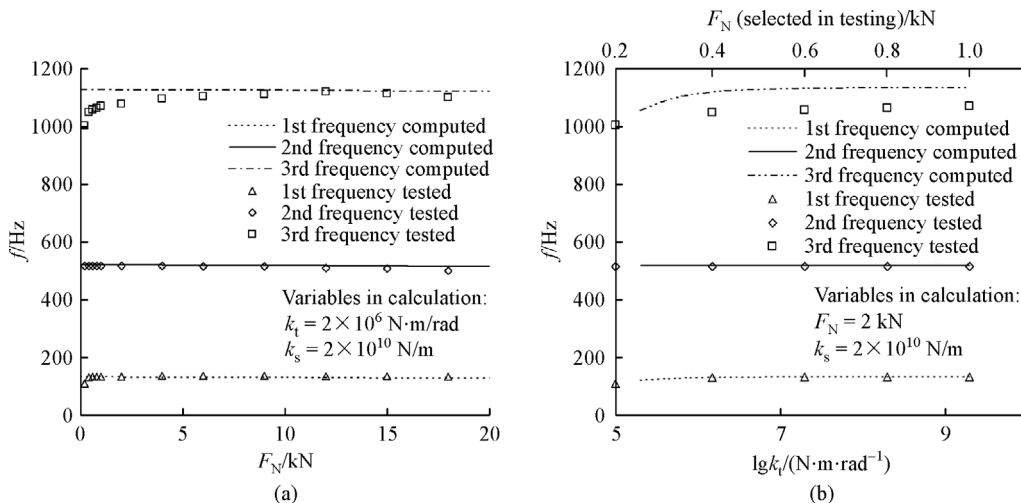


Fig. 11 Frequency comparisons between experimental data and analytical calculations: Results of (a) fixed stiffness and (b) fixed axial loads.

article's Creative Commons license, unless indicated otherwise in a credit line to the material. If material is not included in the article's Creative Commons license and your intended use is not permitted by statutory regulation or exceeds the permitted use, you will need to obtain permission directly from the copyright holder.

To view a copy of this license, visit <http://creativecommons.org/licenses/by/4.0/>.

References

- Pilkey W D, Kang W. Exact stiffness matrix for a beam element with axial force and shear deformation. *Finite Elements in Analysis and Design*, 1996, 22(1): 1–13
- Timoshenko S. *Strength of Materials, Part I: Elementary Theory and Problems*. 2nd ed. New York: D. Van Nostrand, 1940
- Zhang D Y, Fu J W, Zhang Q C, et al. An effective numerical method for calculating nonlinear dynamics of structures with dry friction: application to predict the vibration response of blades with underplatform dampers. *Nonlinear Dynamics*, 2017, 88(1): 223–237
- Qin Z Y, Han Q K, Chu F L. Analytical model of bolted disk-drum joints and its application to dynamic analysis of jointed rotor. *Proceedings of the Institution of Mechanical Engineers, Part C: Journal of Mechanical Engineering Science*, 2014, 228(4): 646–663
- Luan Y, Guan Z Q, Cheng G D, et al. A simplified nonlinear dynamic model for the analysis of pipe structures with bolted flange joints. *Journal of Sound and Vibration*, 2012, 331(2): 325–344
- Song Y X, Hartwigsen C J, McFarland D M, et al. Simulation of dynamics of beam structures with bolted joints using adjusted Iwan beam elements. *Journal of Sound and Vibration*, 2004, 273(1–2): 249–276
- Han F, Dan D H, Cheng W. Exact dynamic characteristic analysis of a double-beam system interconnected by a viscoelastic layer. *Composites. Part B, Engineering*, 2019, 163: 272–281
- Han F, Dan D H, Cheng W. An exact solution for dynamic analysis of a complex double-beam system. *Composite Structures*, 2018, 193: 295–305
- Han F, Dan D H, Cheng W, et al. A novel analysis method for damping characteristic of a type of double-beam systems with viscoelastic layer. *Applied Mathematical Modelling*, 2020, 80: 911–928
- Han F, Zhang Y L, Zang J B, et al. Exact dynamic analysis of shallow sagged cable system—theory and experimental verification. *International Journal of Structural Stability and Dynamics*, 2019, 19(12): 1950153
- Han F, Dan D H, Cheng W, et al. An improved Wittrick-Williams algorithm for beam-type structures. *Composite Structures*, 2018, 204: 560–566
- Paunović S, Cajić M, Karličić D, et al. A novel approach for vibration analysis of fractional viscoelastic beams with attached masses and base excitation. *Journal of Sound and Vibration*, 2019, 463: 114955
- Wu J S, Chang B H. Free vibration of axial-loaded multi-step Timoshenko beam carrying arbitrary concentrated elements using continuous-mass transfer matrix method. *European Journal of Mechanics. A, Solids*, 2013, 38(3): 20–37
- Lin H Y. Dynamic analysis of a multi-span uniform beam carrying a number of various concentrated elements. *Journal of Sound and Vibration*, 2008, 309(1–2): 262–275
- Hong S W, Kim J W. Modal analysis of multi-span Timoshenko beams connected or supported by resilient joints with damping. *Journal of Sound and Vibration*, 1999, 227(4): 787–806
- Yuan Q, Gao R, Feng Z P, et al. Analysis of dynamic characteristics of gas turbine rotor considering contact effects and pre-tightening force. In: *Proceedings of ASME Turbo Expo 2008: Power for Land, Sea and Air*. Berlin: ASME, 2009, 983–988
- Chenaghlou M R, Nooshin H. Axial force-bending moment interaction in a jointing system part I: Experimental study. *Journal of Constructional Steel Research*, 2015, 113: 261–276
- Chenaghlou M R, Nooshin H. Axial force-bending moment interaction in a jointing system part II: Analytical study. *Journal of Constructional Steel Research*, 2015, 113: 277–285
- Yuan S X, Zhang Y Y, Fan Y G, et al. A method to achieve uniform clamp force in a bolted rotor with curvic couplings. *Proceedings of the Institution of Mechanical Engineers, Part E: Journal of Process Mechanical Engineering*, 2016, 230(5): 335–344
- Liu S G, Ma Y H, Zhang D Y, et al. Studies on dynamic characteristics of the joint in the aero-engine rotor system. *Mechanical Systems and Signal Processing*, 2012, 29(5): 120–136
- Failla G, Santini A. On Euler–Bernoulli discontinuous beam solutions via uniform-beam Green's functions. *International Journal of Solids and Structures*, 2007, 44(22–23): 7666–7687
- Failla G, Santini A. A solution method for Euler–Bernoulli vibrating discontinuous beams. *Mechanics Research Communications*, 2008, 35(8): 517–529
- Failla G. Closed-form solutions for Euler–Bernoulli arbitrary discontinuous beams. *Archive of Applied Mechanics*, 2011, 81(5): 605–628
- Failla G, Impollonia N. General finite element description for non-uniform and discontinuous beam elements. *Archive of Applied Mechanics*, 2012, 82(1): 43–67
- Failla G. An exact modal analysis approach to vibration analysis of structures with mass-spring subsystems and rotational joints. *Journal of Sound and Vibration*, 2019, 438: 191–219
- Hei D, Lu Y J, Zhang Y F, et al. Nonlinear dynamic behaviors of a rod fastening rotor supported by fixed-tilting pad journal bearings. *Chaos, Solitons, and Fractals*, 2014, 69: 129–150
- Cui Y M, Fang Z D, Su J Z, et al. Precise modeling of arc tooth face-gear with transition curve. *Chinese Journal of Aeronautics*, 2013, 26(5): 1346–1351
- Zhao N, Li W, Hu T, et al. Quasistatic load sharing behaviours of concentric torque-split face gear transmission with flexible face gear. *Mathematical Problems in Engineering*, 2018, 6568519
- Works G. Curvic coupling design. *Gear Technology*, 1986, 3(6): 34–48
- Richardson I J, Hyde T M, Becker A A, et al. A three-dimensional finite element investigation of the bolt stresses in an aero-engine curvic coupling under a blade release condition. *Journal of Aerospace Engineering*, 2000, 214(4): 231–245
- Lee J W, Lee J Y. An exact transfer matrix expression for bending vibration analysis of a rotating tapered beam. *Applied Mathematical Modelling*, 2018, 53: 167–188
- Patil D P, Maiti S K. Detection of multiple cracks using frequency

- measurements. *Engineering Fracture Mechanics*, 2003, 70(12): 1553–1572
33. Dan D H, Han F, Cheng W, et al. Unified modal analysis of complex cable systems via extended dynamic stiffness method and enhanced computation. *Structural Control Health Monitoring*, 2019, 26(10): e2435
 34. Hong J, Chen X Q, Wang Y F, et al. Optimization of dynamics of non-continuous rotor based on model of rotor stiffness. *Mechanical Systems and Signal Processing*, 2019, 131(15): 166–182
 35. Iranzad M, Ahmadian H. Identification of nonlinear bolted lap joint models. *Computers & Structures*, 2012, 96–97(4): 1–8
 36. Timoshenko S. *Vibration Problems in Engineering*. 2nd ed. New York: D. Van Nostrand, 1937
 37. Wang L, Yu M C. Effect of axial force on the lateral vibration characteristics of Timoshenko beam under free boundary condition. *Journal of Ordnance Equipment Engineering*, 2018, 39: 36–39 (in Chinese)
 38. Bronshtein I, Semendyayev K, Musiol G, et al. *Handbook of Mathematics*. Berlin: Springer, 2015: 949–1022
 39. Genta G. *Dynamics of Rotating Systems*. New York: Springer, 2005
 40. Liu H, Hong J, Shao F Y, et al. Progress and prospect of structural design and processing technology of curvic coupling. *Journal of Propulsion Technology*, 2018, 39(4): 1–10 (in Chinese)
 41. Xiang T, Lan D, Zhang S, et al. Experimental modal test of the spiral bevel gear wheel using the PolyMAX method. *Journal of Mechanical Science and Technology*, 2018, 32(1): 21–28